SAND2021-12192C

Here Comes the Suns – Flight Safety for Unmanned Aircraft Systems Over Active Heliostat Fields

David K. Novick[a)], Randy C. Brost, Daniel E. Small,
Noah R. Jackson, and Micah Mann

Sandia National Laboratories
P.O. Box 5800
Albuquerque, NM 87185 USA

[a)] *dknovic@sandia.gov*

Abstract. The freedom of flight allows unmanned aircraft systems (UAS) the ability to inspect large areas without the necessity of roads or other types of infrastructure. This is a very desirable trait when several thousands of mirrors require inspection. Operational concentrating solar power plants generate regions of high solar flux. These unseen areas present potential flights hazards to the UAS. The intensity of these areas over the field needs to be understood, as well as how these affect the flight of a UAS. How much flux can a UAS endure before it fails? Understanding this will allow a safe flight path to be generated to avoid these failures. In a first experiment, a DJI Phantom 3 (painted black) was subjected to six suns total irradiance. The internal and external temperatures were logged and analyzed. No internal or external damage to the UAS was observed.

INTRODUCTION

Concentrating solar power (CSP) plants often have several thousand mirrors with associated support and actuation mechanisms spread over a large land area. Tuning, inspection, and maintenance of such large systems is a daunting challenge. As a result, unmanned aircraft systems (UASs) have received increased attention as an appealing potential option for CSP inspection tasks, because they can move a camera or other inspection sensors systematically across large solar field areas [1] [2] [3].

However, an operating CSP field has varying regions of high solar flux, which can present a potential flight hazard. This is not an acute problem for parabolic trough, dish Stirling, or linear Fresnel plants, because their regions of high flux are spatially localized to small areas that are close to hardware components and thus generally avoided by UAS flights. For heliostat fields, the region of solar flux is widespread, and UASs flying over an operating heliostat will inherently encounter areas of increased solar flux. Irradiance intensities near the receiver may reach 3,000 kW/m^2, which can cause immediate spontaneous combustion in many materials.

UAS vehicles are vulnerable to high temperature damage. For example, lithium-polymer (LiPo) batteries are subject to thermal runaway due to either electro-mechanical damage or high temperatures [4]. This has led to fire incidents; see [5] for an example. Other types of UAS that use liquid petroleum fuels could be similarly vulnerable. Additional potential mechanisms for UAS damage include thermal-induced malfunction of electronic controls, sensor damage, or permanent damage to the drone fuselage through thermoplastic deformation.

As the use of UASs becomes more prevalent around concentrated solar power plants, these effects must be understood so that safe trajectories can be generated to avoid potential UAS damage. This paper investigates the question: How can we conduct flight operations over an active heliostat field while avoiding hazardous conditions due to solar flux? We explore the problem in two parts: (1) Characterizing the solar flux intensity over the solar field via simulation, and (2) Identifying solar flux intensity levels compatible with safe UAS flight operations.

SOLAR FLUX INTENSITY

Heliostats are designed to focus sunlight onto a central receiver. The beam reflected from a heliostat becomes narrower due to the focusing effect of the heliostat's curvature and becomes broader due to the effect of the sun's finite diameter. In many situations, the overall beam becomes narrower, reaching a maximum flux intensity at the focal point. Since the reflected beam diameter varies linearly with the distance from the heliostat, the flux intensity grows with the square of this distance.

Figure 1 illustrates this effect. In part (a) of the figure, the heliostat mirror has area A_m and due to heliostat focus, this narrows to a beam of area A_r on the receiver. Neglecting the gradual transition in beam shape from the rectangular heliostat to the circular beam spot on the receiver, the width of the beam varies linearly from the heliostat to the receiver at distance d_{mr} from the heliostat. The area A_s of a section of the beam therefore varies with the square of the distance d from the mirror to the section of interest. Figure 1(b) demonstrates how this same effect applies when viewing sections taken along a constant-altitude plane. The section area A_h varies with the square of the altitude z as it increases from z_m to z_r. Since the power in the beam is conserved (neglecting atmospheric attenuation effects), the flux intensity in kW/m^2 therefore grows with the square of either the distance from the mirror d or the altitude z.

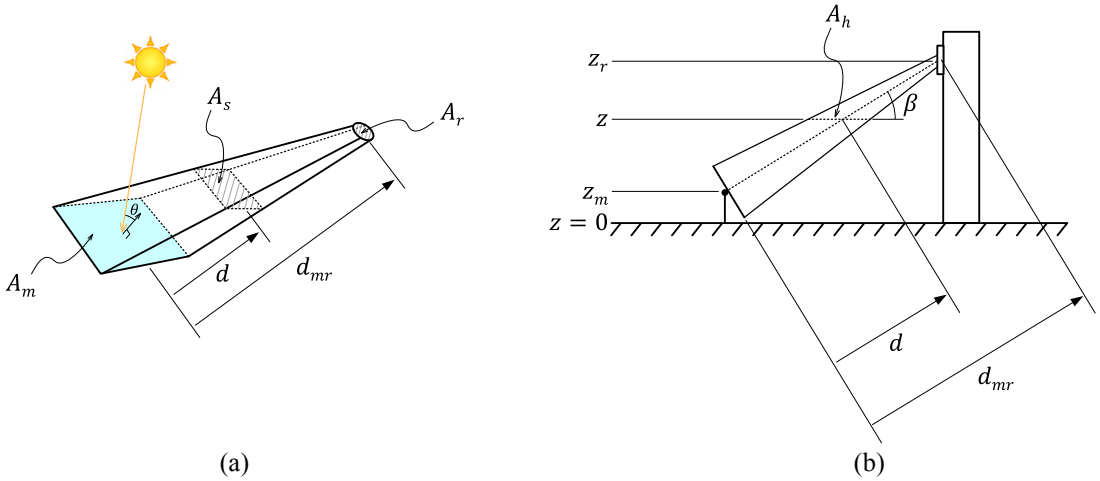

FIGURE 1. A model of flux intensity based on conservation of power.

Similar reasoning applies to the ensemble of reflected beams over a heliostat field. We can view the ensemble of heliostats as a monolithic mirror and observe that the total reflected beam transitions from an initial total mirror area corresponding to the sum of all heliostat areas[1], to a much smaller area at the focus point of maximum concentration. This yields a simple first-order model of the flux intensity over an operating solar field as a function of altitude.

The blue dashed curve in Figure 6 shows a plot of the resulting flux intensity estimate as a function of altitude over the Sandia National Solar Thermal Test Facility (NSTTF) solar field. Notice how the flux intensity grows slowly at first, and then rapidly increases at higher altitudes. This suggests a UAS data collection strategy designed around low-altitude flight, to avoid regions of high flux.

We can refine our understanding by constructing detailed flux intensity maps using ray tracing. Toward this end, we constructed a model revealing the three-dimensional structure of the flux field over the Sandia NSTTF. We produced the model using Monte-Carlo raytracing in SolTrace. Figure 2 shows the layout of the NSTTF solar field. We modeled the heliostats as single surface parabolic reflectors with area equal to 6.096 m × 6.096 m, reflectivity of 88.5% and slope error of 1.2 milliradians.[2]

Figure 3 shows the ray tracing situation we studied. The simulation assumes spring equinox, solar noon, and NSTTF latitude. The sun shape is a pillbox subtending 4.65 milliradians. We configured the solar field to track the heliostats to an aim point at (60 m, 8 m, 28.8 m), relative to the NSTTF origin at the base of the tower (see Figure 2). The simulation traced 25 million rays.

---

[1] In this simple first-order analysis, we neglect the effects of blocking and shading, which may reduce the flux intensity.

[2] The heliostat reflective area in our simulation is greater than the actual heliostat reflective area because we do not model the gaps between mirror facets.

We added sample planes to the model to characterize the flux intensity at different altitudes. Figure 4 shows a side profile of the analysis. In the figure, north is right, zenith is up, and east is coming out of the page. Horizontal sample planes at elevations 10, 14, 15, 16, 17, 18, 19, 20, 21, 22, 23, 24, 25, 26, 26.5, 27, 27.5, 28.3, 28.8, 29, 29.5, 30, 30.5, 31, 31.5, 32, 32.5, and 33 meters were placed to record the hits from the reflected sunlight coming from the heliostat field. As seen in Figure 4, the sample planes initially have low density right above the heliostat field, but sample at a much finer resolution near the focus altitude of 28.8 m, because this is where we expect the flux to change rapidly. Given the simulation's 25 million rays, each of the 216 heliostats is hit by about 102,000 sun rays.

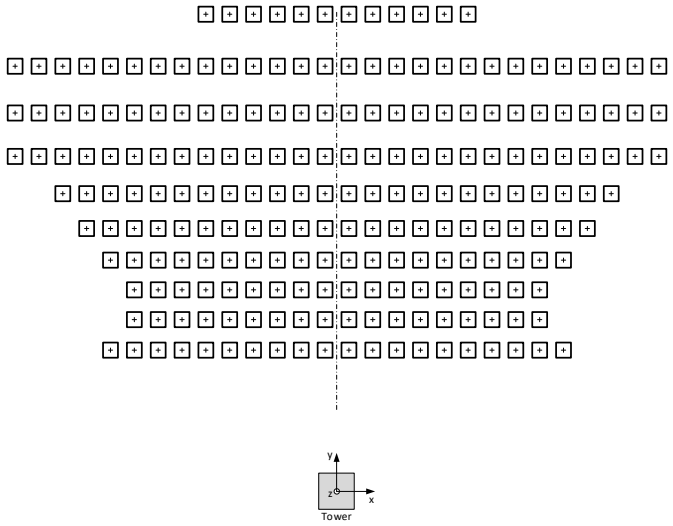

FIGURE 2. Sandia NSTTF solar field layout, drawn to scale.

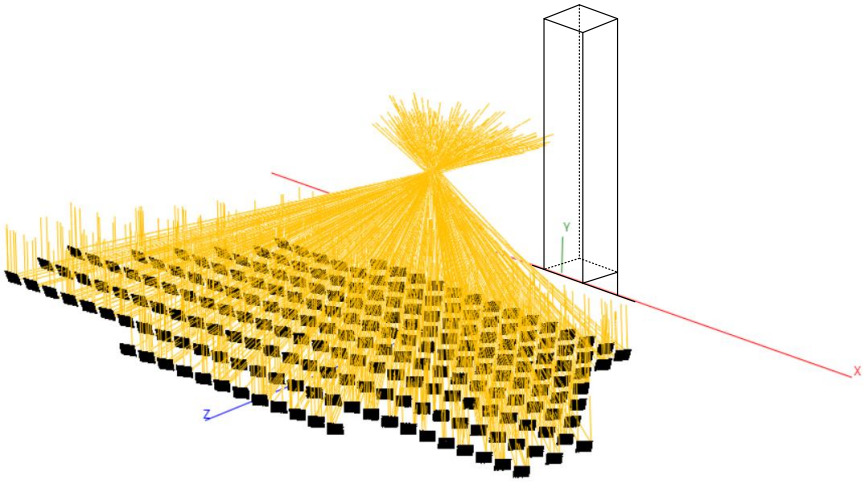

FIGURE 3. Ray-tracing model of Sandia NSTTF tracking to the standby aim point (60, 8, 28.8) meters.

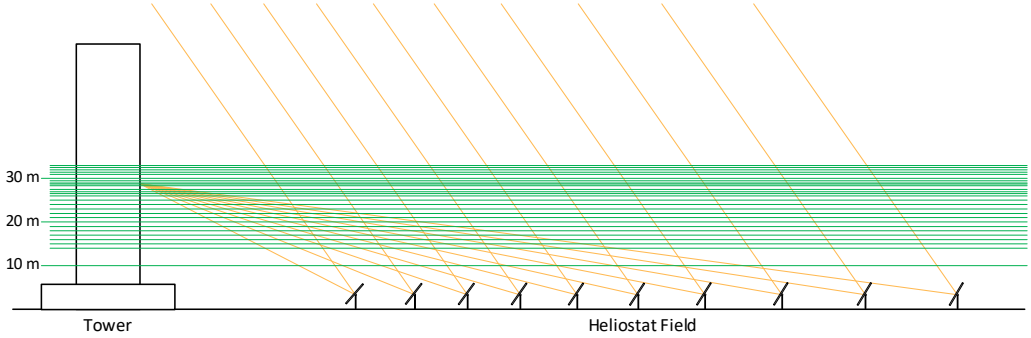

FIGURE 4. Ray-tracing *z* sample planes, drawn to scale.

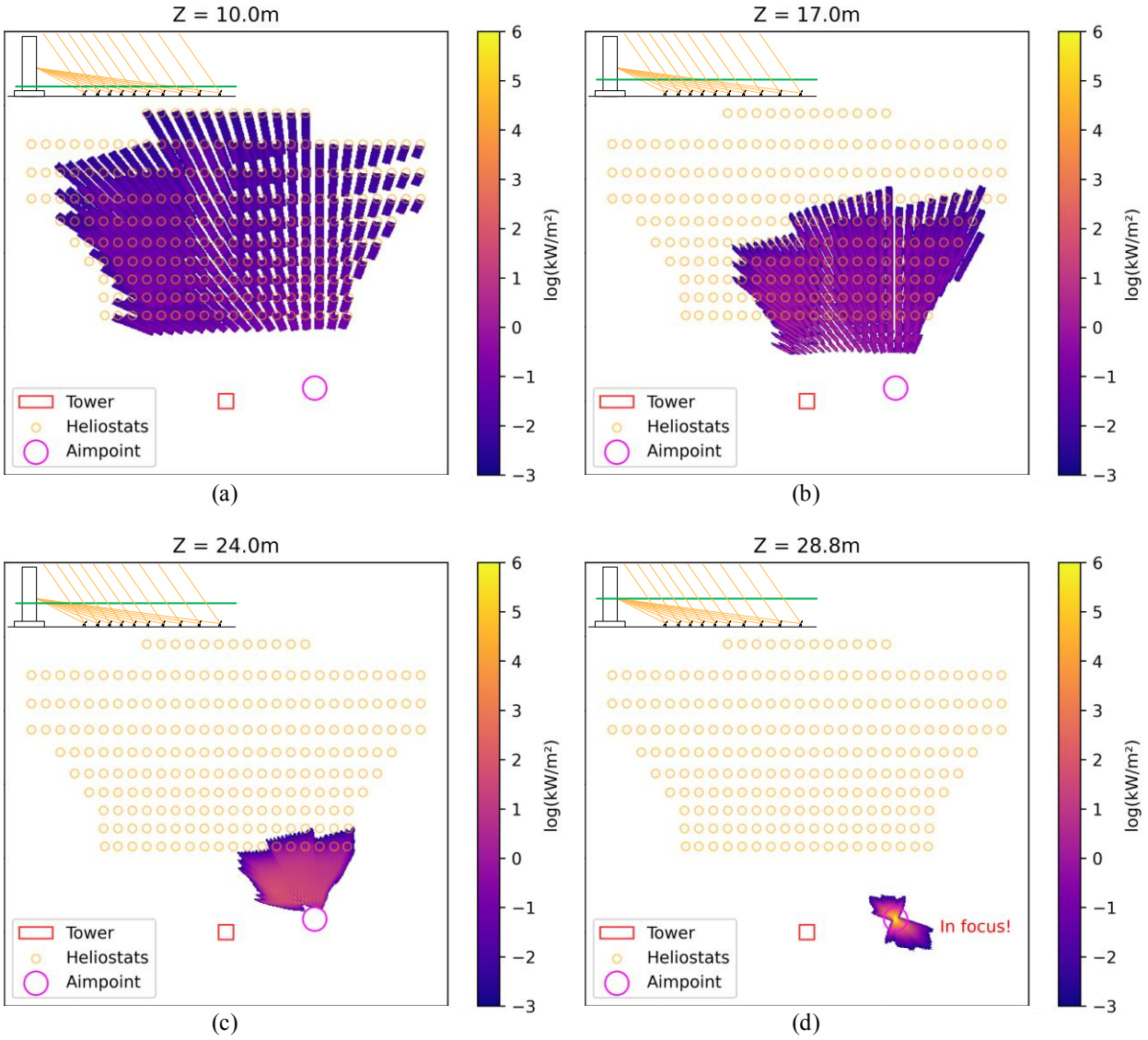

FIGURE 5. Ray-trace intensity at four example *z* sample planes. Note the log scale.

Figure 5 and Figure 6 show simulation results. Figure 5 shows the flux intensity measured at four different example altitudes; note that the colors are drawn to a log scale. The diagram inset in the upper left of each subfigure shows the cross-section of Figure 4, but with the particular sample plane highlighted in green. Part (a) shows the first altitude $z = 10$ m. This altitude is close to the heliostats; individual shapes are easily recognized in the flux pattern. Parts (b) and (c) show intermediate altitudes; notice that the flux intensity increases with altitude, as reflections from individual heliostats both become individually tighter and merge together. Part (d) shows the maximum flux at the $z = 28.8$ m focal point altitude, where all of the reflected power is concentrated into a very small spatial area. Notice that the flux increase is very dramatic with the final increase in altitude (remember the log scale). Sample planes at higher altitudes show the flux dispersing in a pattern much like the altitudes preceding the focus altitude (not shown).

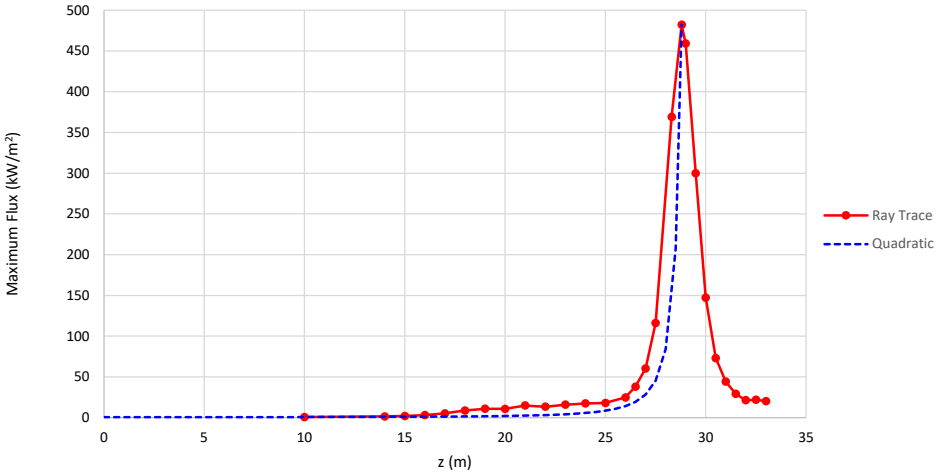

FIGURE 6. Predictions of flux intensity as a function of altitude over the Sandia NSTTF solar field. Note that intensity is measured in a horizontal plane, which reduces the reported intensity. See text.

Figure 6 shows a plot of the maximum flux intensity. The red curve shows the maximum ray-tracing flux recorded in each sample plane as a function of sample plane elevation. The peak flux uncertainty was less than 3% reported from SolTrace as a function of data export parameters like field size, a 512 x 512 bin resolution, and 50 contour lines. The blue dashed curve shows a quadratic function corresponding to our first-order model of the variation in flux with altitude. The maximum flux is set to match the ray-tracing result to enable comparison of the curve shapes. The ray tracing peak flux follows the quadratic curve closely; the points where the peak ray-tracing flux is higher may be due to local hot spots resulting from overlap between closely adjacent heliostats.

The reflected ray-tracing beams strike the horizontal sample plane at an average oblique angle β of about 13° (see Figure 1(b)). As a result, the vertical axis values of Figure 6 are reduced by a factor of about $\sin(\beta) \approx 0.2$ times the values that would be measured by a sample plane perpendicular to the reflected beams. Thus by this estimate, a UAS presenting surface perpendicular to the flux would receive about 2,200 kW/m^2 irradiance at the focal point!

EXPLORING SAFE OPERATION LIMITS

We could use this model of flux intensity to plan safe UAS flights, but first we must answer another question: How much flux can the UAS safely tolerate? This question may be explored either analytically or experimentally. Because of the high complexity of UAS systems and the difficulty of producing an accurate analytic model, we chose an experimental approach.

A DJI Phantom 3 was painted black to increase solar absorption, and three iButton [6] temperature sensors were placed on the aircraft top, bottom, and inside the battery compartment (Figure 7(a)). A reference sensor was placed on a table in direct sunlight. Battery temperature and electronic speed controller (ESC) temperature were extracted from flight logs. Heliostat mirrors were manually directed to reflect multiple suns on the aircraft (Figure 8).

Conditions ranged from overcast to reflecting five mirrors onto the UAS, resulting in total irradiance varying from zero to six suns. Figure 8 shows the case with five reflected mirrors plus overhead irradiance, approximating six suns. The two plots in Figure 9 show the reference sensor reading. The insolation was significantly lower in the six sun case due to partly cloudy weather conditions. Despite this, the six-sun plot exhibits higher and faster-rising ESC temperatures. No damage to the UAS was observed. Note that ambient temperature was cool (approximately 10 °C), and a breeze up to 7 km/h provided convective cooling.

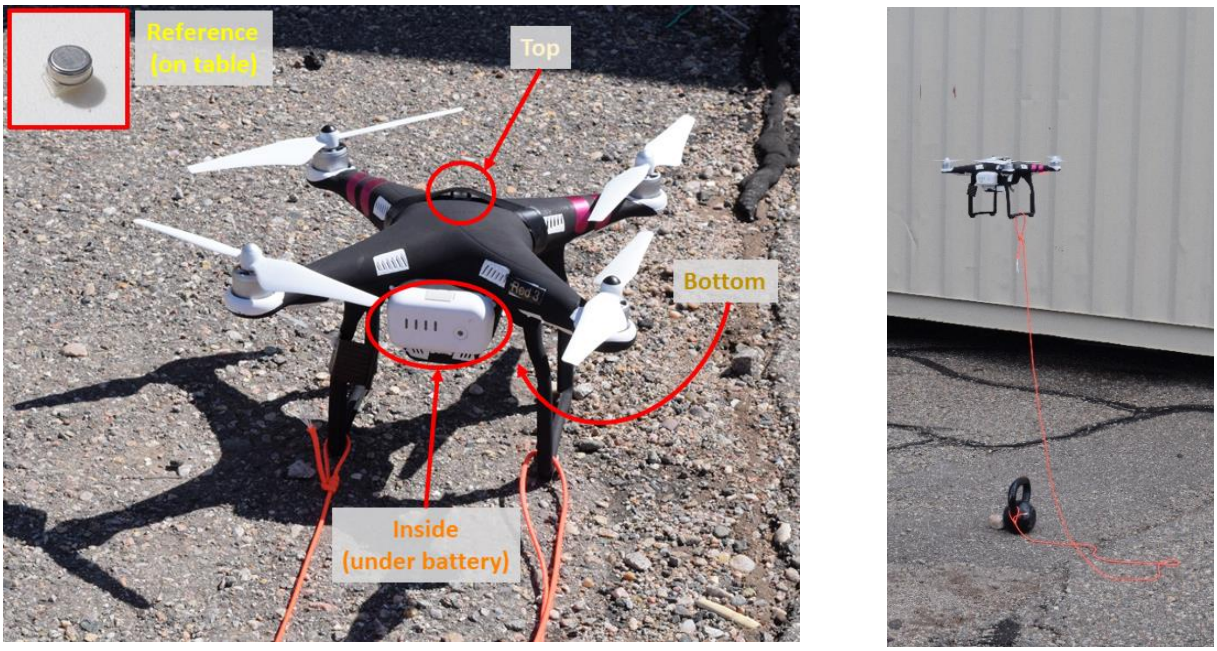

(a) (b)

FIGURE 7. UAS setup.

Figure 7(a) shows the distribution of the temperature sensing on and in the UAS. Figure 7(b) shows the UAS attached to a short piece of 550 pound-test paracord, with the ground side attached to a 20-pound kettle bell. The drone was attached to the kettle bell as a precaution in case it were to behave uncontrollably due to high heat.

FIGURE 8. Flight test with six suns irradiance (5 mirrors plus 1 overhead).

Figure 8 shows five members of the team manually directing solar flux from each mirror onto the UAS. This flight was a first step within a larger ongoing experimental campaign designed to push the UAS up to and past its operating limits to determine exactly where those limits are.

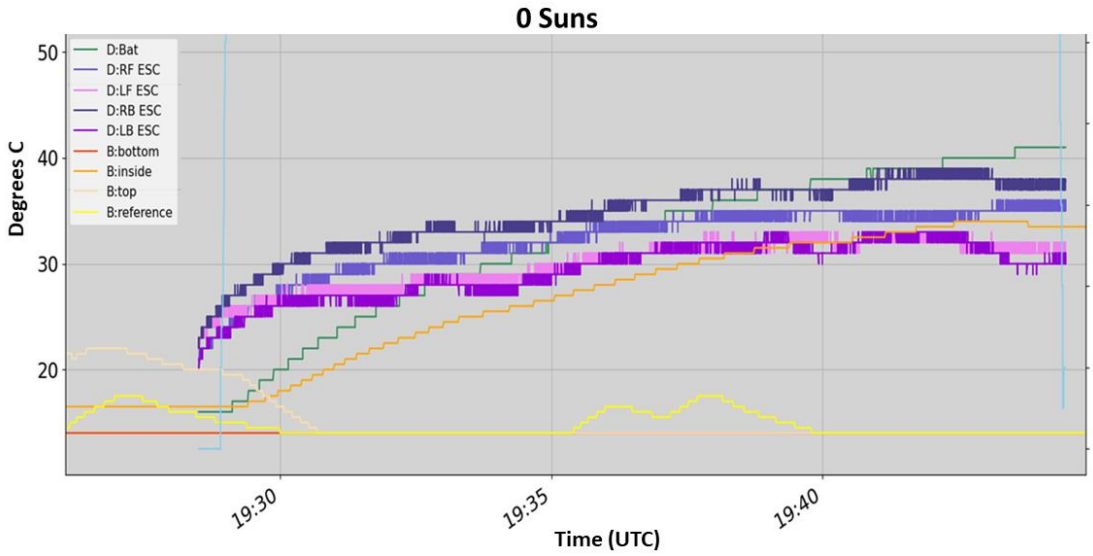

(a)

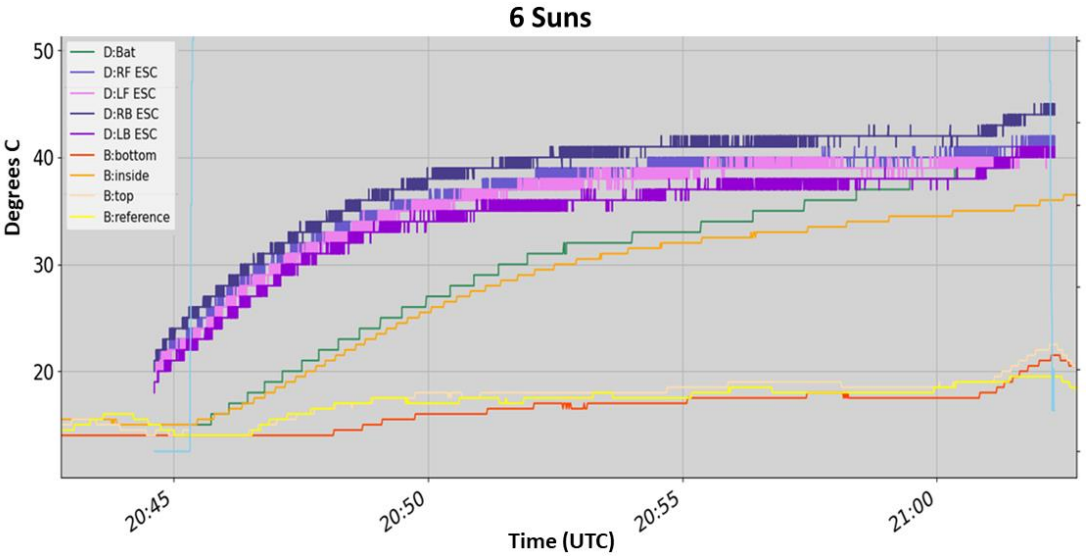

(b)

FIGURE 9. Graph of temperature versus time.

Figure 9 above shows graphs of temperature versus time. Both figures plot the temperature sensors from both the UAS logs (battery and the four electronic speed controller temperatures) and the button sensors (bottom, inside, top, and reference). The thin blue vertical lines at the start and end of each graph represent landing and takeoff times. The time axis is reported as UTC and the offset for Albuquerque is -7 hours.

FLIGHT EXPERIENCE

This work is part of a larger effort to develop UAS-based techniques for measurement and inspection of large-scale heliostat fields [3]. In addition to the above experiment where we intentionally exposed a UAS to concentrated sunlight, in the course of this work we have also flown 45 flights over active solar fields, collecting post-flight temperature data of the drone top, bottom, and battery compartment. Solar field configurations varied from

concentrating configurations, such as the configuration shown in Figures 3-6[3], to more dispersed heliostat aiming configurations. UAS flight altitudes at the Sandia NSTTF ranged from 13 m to 30 m above the z=0 reference point at the base of the tower; however, all flights maintained significant altitude clearance below the concentration aim point or avoided the focus area laterally. Post-flight observed UAS temperatures did not exceed 57 °C; for a given flight, the highest temperature was generally observed inside the battery compartment.

It's worth noting that the experiment logged both internal and external temperatures in excess of 40 °C, which is the upper limit for the published temperature spec for this system. Future experiments along these lines are likely to significantly exceed this boundary.

DISCUSSION

Note that this is just one type of drone. While we have painted it flat black to approximate a worst-case scenario with regard to solar absorption, other factors in drone construction may also come into play, including a system's ability to actively (internal fans) and passively (white/reflective paint on the bottom, external heatsinks) cool itself, or the opposite condition where heat builds up quickly.

A key lesson learned is to plan paths that favor low altitudes and avoid regions of high flux concentration. We note that for very large solar fields such as full-size commercial power plants, a lateral avoidance strategy may not be an option.

Additional hazards include intense reflected light from either the sun or the receiver heating the camera sensor; this concern is more significant for cameras which do not include a shutter or single-lens reflex mirror to protect the sensor. This topic merits further study but is beyond the scope of this paper.

ACKNOWLEDGMENTS

We thank Lam Banh, Roger Buck, Luis Garcia Maldonado, and Rip Winckel for their assistance with the flight test. We also thank the DOE Solar Energy Technologies Office for their support. Sandia National Laboratories is a multimission laboratory managed and operated by National Technology & Engineering Solutions of Sandia, LLC, a wholly owned subsidiary of Honeywell International Inc., for the U.S. Department of Energy's National Nuclear Security Administration under contract DE-NA0003525.

REFERENCES

[1] R. Mitchell and G. Zhu, "A Non-Intrusive Optical (NIO) Approach to Characterize Heliostats in Utility-Scale Power Tower Plants," *Solar Energy 209,* pp. 431-445, 2020.

[2] J. Yellowhair, P. Apostolopoulus, D. Small, D. Novick and M. Mann, "Developement of an Aerial Imaging System for Heliostat Canting Assessments," in *SolarPACES*, 2020.

[3] R. Brost, P. Apostolopoulos, D. Small, D. Novick, N. Jackson, M. Mann and E. Tsiropoulou, "High-Speed In Situ Optical Scanning of Heliostat Fields," in *SolarPACES*, 2021.

[4] H. Barkholtz, Y. Preger, S. Ivanov, J. Langendorf, L. Torres-Castro, J. Lamb, B. Chalamala and S. Ferreira, "Multi-scale thermal stability study of commercial lithium-ion batteries as a function of cathode chemistry and state-of-charge," *Journal of Power Sources 435*, 2019.

[5] B. Gabbert, "Drone crash starts fire in Oregon," *Wildfire Today,* 11 July 2018.

[6] iButtonLink, "iButtonLink Technology," [Online]. https://www.ibuttonlink.com/collections/thermochron. Accessed September 26, 2021.

[3] Some heliostats were offline during our flights, reducing the total irradiance. The number of offline heliostats varied. The concentration aim point *z* value also varied between 28.8 m to 60 m.